Res. Commun. 126, 178–184.
Garcia, R., Cantin, M., DeLean, A., Genest, J., Godin, G., Gutkowska, J., Schiffrin, E. L., & Thibault, G. (1986) *Biochem. Biophys. Res. Commun. 135*, 987–993.
Glembotski, C. C., & Gibson, T. R. (1985) *Biochem. Biophys. Res. Commun. 132*, 1008–1017.
Glembotski, C. C., Wildey, G. M., & Gibson, T. R. (1985) *Biochem. Biophys. Res. Commun. 129*, 671–678.
Habener, J. F., Kronenberg, H. M., & Potts, J. T. (1981) *Methods Cell Biol. 23*, 51–71.
Hjort, P., Rapapport, S., & Owren, P. A. (1955) *J. Lab. Clin. Med. 46*, 89–93.
Kangawa, K., Tawaragi, Y., Oikawa, S., Mizuno, A., Sakuragawa, Y., Nakazato, H., Fukada, A., Minamino, N., & Matsuo, H. (1984) *Nature (London) 312*, 152–155.
Laemmli, U. K. (1970) *Nature (London) 227*, 680–685.
Lottenberg, R., Christensen, U., Jackson, C. M., & Coleman, P. L. (1981) *Methods Enzymol. 80*, 341–364.
Lowry, O. H., Rosebrough, N. J., Farr, A. L., & Randall, R. J. (1951) *J. Biol. Chem. 58*, 265–275.
Maki, M., Takayanagi, R., Misono, K. S., Paudey, K. N., Tibbetts, C., & Inagami, T. (1984) *Nature (London) 309*, 722–724.
Miyota, A., Kangawa, K., Tashimori, T., Hatch, T., & Matsuo, H. (1985) *Biochem. Biophys. Res. Commun. 129*, 248–255.
Osterud, B., & Flengsrud, R. (1975) *Biochem. J. 145*, 469–474.
Schwartz, D., Geller, D. M., Manning, P. T., Seigel, N. R., Fok, K. R., Smith, C. E., & Needleman, P. (1985) *Science (Washington, D.C.) 229*, 397–400.
Seidman, C. E., Duby, A. D., Choi, E., Graham, R. M., Haber, E., Homcy, C. J., Smith, J. A., & Seidman, J. G. (1984) *Science (Washington, D.C.) 225*, 324–326.
Sugarawa, A., Nakao, K., Morii, N., Sakamoto, M., Suda, M., Shimokura, M., Kiso, Y., Kihara, M., Yamori, Y., Nishimura, K., Soneda, J., Ban, T., & Imura, H. (1985) *Biochem. Biophys. Res. Commun. 129*, 439–446.
Tager, H. S., Steiner, D. F., & Patzelt, C. (1981) *Methods Cell Biol. 23*, 73–88.
Thibault, G., Garcia, R., Carrier, F., Seidah, N. G., Lazure, C., Cantin, M., & Genest, J. (1984) *Biochem. Biophys. Res. Commun. 125*, 938–946.
Thibault, G., Lazure, C., Schiffrin, E. L., Gutkowska, J., Chartier, L., Garcia, R., Seidah, N. G., Chretien, M., Genest, J., & Cantin, M. (1985) *Biochem. Biophys. Res. Commun. 130*, 981–986.
Trippodo, N. C., Januszewicz, A., Pegram, B. L., Cole, F. E., Kahashi, N., Kardon, M. B., MacPhee, A. A., & Frohlich, E. D. (1985) *Hypertension 7*, 905–912.
Vuolteenaho, O., Arjamaa, O., & Ling, L. (1985) *Biochem. Biophys. Res. Commun. 129*, 82–88.
Yamaji, T., Ishibashi, M., & Takaku, F. (1985) *J. Clin. Invest. 76*, 1705–1709.
Yamanaka, M., Greenberg, B., Johnson, C., Seilhammer, J., Brewer, M., Friedmann, T., Miller, J., Atlas, S., Laragh, J., Lewicki, J., & Fiddes, J. (1984) *Nature (London) 309*, 719–722.
Zisfein, J. B., Matsueda, G. R., Fallon, J. T., Bloch, K. D., Seidman, C. E., Seidman, J. G., Homcy, C. J., & Graham, R. M. (1986a) *J. Mol. Cell. Cardiol. 18*, 917–929.
Zisfein, J. B., Bloch, K. D., Sylvestre, D., Margolies, M. N., Seidman, J. G., Homcy, C. J., & Graham, R. M. (1986b) *Circulation 74*, II–462.

Hinging of Rabbit Myosin Rod†

M. E. Rodgers* and W. F. Harrington
Department of Biology and McCollum-Pratt Institute, The Johns Hopkins University, Baltimore, Maryland 21218
Received November 3, 1986; Revised Manuscript Received August 24, 1987

ABSTRACT: The question of hinging in myosin rod from rabbit skeletal muscle has been reexamined. Elastic light scattering and optical rotation have been used to measure the radius of gyration and fraction helix, respectively, as a function of temperature for myosin rod, light meromyosin (LMM), and long subfragment 2 (long S-2). The radius of gyration vs temperature profile of myosin rod is shifted with respect to the optical rotation melting curve by about −5 °C. Similar studies on both LMM and long S-2 show virtually superimposable profiles. To correlate changes in the secondary structure with the overall conformation, plots of radius of gyration vs fraction helix are presented for each myosin subfragment. Myosin rod exhibits a marked decrease in the radius of gyration from 43 nm to ~35 nm, while the fraction helix remains at nearly 100%. LMM and long S-2 did not show this behavior. Rather, a decrease in the radius of gyration of these fragments occurred with comparable changes in fraction helix. These results are interpreted in terms of hinging of the myosin rod within the LMM/S-2 junction.

It is generally believed that force generation and shortening in a contracting muscle are a result of the cyclic attachment and detachment of cross-bridges between neighboring thick and thin filaments concomitant with the hydrolysis of ATP. The ultimate goal of research on muscle contraction is to understand the events of the cross-bridge cycle at the molecular level. Most of the current models of contraction which attempt to provide a molecular mechanism include two flexible regions in the myosin molecule: one between each myosin head (subfragment 1) and the coiled-coil α-helical rod and a second located near the center of the rod. The swivellike joint between myosin subfragment 1 (S-1)[1] and the rod of myosin provides

† Supported by National Institutes of Health Grant AM-04349 (to W.F.H.) and by a Muscular Dystrophy Association postdoctoral fellowship (to M.E.R.). This is Contribution No. 1386 from the McCollum-Pratt Institute of The Johns Hopkins University.
* Address correspondence to this author at the Department of Biology, The Johns Hopkins University.

0006-2960/87/0426-8697$01.50/0

for nearly unrestricted motion of the head. The high flexibility of this region has been demonstrated both in solution and in the assembled thick filament [reviewed by Harvey and Cheung (1982)]. The so-called hinge region in the center of the myosin rod, however, has been the subject of some controversy. In the rotating head model, the hinge has been postulated to allow the cross-bridge to swing away from the thick filament surface during a cross-bridge cycle, so that S-1 can interact with actin (Huxley, 1969; Huxley & Simmons, 1971). Some type of structural transition in the actin-attached myosin head is believed to generate the contractile force at all interfilament spacings as the filaments slide past each other in a contracting muscle. In the helix–coil model, the hinge is postulated to be the primary site of force generation and shortening (Harrington, 1971, 1979). During the contractile cycle, the hinge region undergoes a reversible helix–coil transition following release of the actin-attached cross-bridge from the thick filament surface.

A number of studies have addressed the question of hinging of the myosin molecule both in the assembled thick filament and in myosin in solution [see review by Harvey and Cheung (1982)]. One of the earliest indications of instability of the hinge region came from proteolytic susceptibility studies on myosin (Mihalyi & Harrington, 1959). More recent proteolysis studies on myosin, intact myofibrils, and muscle fibers are consistent with the earlier results and demonstrate further that the proteolytic susceptibility of this region is markedly increased upon activation of (rabbit) skeletal muscle (Ueno & Harrington, 1986a,b). In addition, the lower thermal stability of the hinge region has been supported by differential scanning calorimetry (Swenson & Ritchie, 1980), electric birefringence (Highsmith et al., 1977; Bernengo & Cardinaud, 1982), temperature-jump experiments (Tsong et al., 1979, 1983), and analysis of the amino acid sequence (Lu & Wong, 1985; Strehler et al., 1986). Electron microscopic studies have also demonstrated two distinct bending points in myosin, one at about 44 nm (Elliott & Offer, 1978; Walker et al., 1985) and a second at 76 nm (Takahashi, 1978; Walker et al., 1985) from the head–tail junction. These loci encompass the region of high proteolytic susceptibility described by Ueno and Harrington (1984a,b). On the other hand, a number of physicochemical studies have obtained opposing results. Electric birefringence (Hvidt et al., 1984), viscoelastic (Rosser et al., 1978), and fluorescence depolarization (Harvey & Cheung, 1977) measurements suggest that myosin rod behaves as a rather rigid molecule in solution.

In the work described below, we have reexamined the question of hinging in the myosin rod and its principle proteolytic fragments light meromyosin (LMM) and subfragment-2 (S-2), using optical rotation to monitor changes in the secondary structure and elastic light scattering to determine corresponding changes in the radius of gyration as a function of temperature. As is well-known [e.g., see Yu and Stockmayer (1967)], the radius of gyration is a sensitive indicator of hinging within the structure of rodlike molecules.

Materials and Methods

Reagents. α-Chymotrypsin and papain were purchased from Worthington Biochemicals. α-Chymotrypsin (3× recrystallized) was further treated with TLCK (tosyl-L-lysine chloromethyl ketone) as described by Shaw et al. (1965) to remove any trypsin contaminant. Trypsin, soybean trypsin inhibitor, dithiothreitol (DTT), iodoacetamide, and phenylmethanesulfonyl fluoride (PMSF) were obtained from Sigma Chemical Co. Ammonium sulfate (ultrapure) was obtained from Schwarz/Mann. Hydroxylapatite (Bio-Gel HT) was purchased from Bio-Rad, and Sephacryl S-300 and S-400 were from either Pharmacia or Sigma Chemical Co. All reagents used in this study were reagent grade or better.

Proteins. Myosin was isolated according to the procedure of Godfrey and Harrington (1970). The various LMM and S-2 fragments were obtained from myosin as described below.

Myosin rod was prepared by papain digestion of myofibrils and purified according to the method of Hvidt et al. (1982). LMM was prepared by digestion of myosin (18 mg/mL) in buffer M (0.6 M NaCl, 20 mM PO_4^{2-}, 1 mM EDTA, and 0.5 mM DTT, pH 7.0) + 2 mM $CaCl_2$ with α-chymotrypsin (0.1 mg/mL) for 4 h at 0 °C. The digestion was quenched by addition of 1 mL of PMSF (15 mg/mL in absolute EtOH) per 100 mL of solution. The resulting mixture was dialyzed overnight versus 20 mM imidazole, pH 6.2, to precipitate LMM and any undigested myosin and then centrifuged at high speed (80000*g* for 20 min). The supernatant, containing long HMM (Sutoh et al., 1978), was retained for preparation of subfragment 2 as described later; the pellet was resuspended in buffer M. Three volumes of ethanol were added slowly to denature the undigested myosin and precipitate all of the protein. The precipitate was collected by centrifugation as above, and LMM was recovered from the pellet by resuspension in buffer M, dialysis against buffer M, and centrifugation to remove material which did not redissolve. The LMM was then subjected to two cycles of isoelectric precipitation (using acetic acid to drop the pH to 4.6) followed by resuspension in buffer M. The final pellet was redissolved in 0.5 M KCl, 25 mM potassium phosphate (pH 7.0), and 2 mM DTT and chromatographed on hydroxylapatite as described by Hvidt et al. (1982).

Long S-2 was prepared from long HMM by chymotryptic digestion in the absence of divalent cation according to the procedure of Sutoh et al. (1978). Long HMM, obtained by chymotryptic digestion as described above, was precipitated by the addition of 1.5 volumes of saturated ammonium sulfate and 10 mM EDTA, pH 6.8. The precipitate was collected by centrifugation at 12000*g* for 15 min, redissolved in buffer M + 1 mM DTT, and dialyzed against the same solvent. Long HMM (10 mg/mL) was digested with α-chymotrypsin (0.25 mg/mL) for 20 min at 4 °C, the digestion quenched by addition of PMSF, and the resulting mixture of proteins precipitated by addition of 3 volumes of ethanol. Following centrifugation, S-2 was recovered by resuspension of the pellet in buffer M followed by dialysis and centrifugation to remove denatured material. This S-2 preparation contained a mixture of 61K, 53K, and 34K fragments. The two high molecular weight fragments were precipitated from solution by addition of $CaCl_2$ as described by Ueno et al. (1983). In a final step, the 61K and 53K fragments were separated from each other by repeated chromatography on Sephacryl S-300.

Optical Rotation. A Cary 60 spectropolarimeter was employed for optical rotation measurements as described by Sutoh et al. (1978). Rotation was measured at the Cotton trough minimum (λ = 231.4 nm) using a 1-cm path length, water-jacketed cell. Temperature was controlled by use of an external circulating bath. We measured rotation at 1- or 2-deg increments in temperature between 2 and 80 °C to obtain

[1] Abbreviations: S-1, myosin subfragment 1; LMM, light meromyosin; HMM, heavy meromyosin; S-2, myosin subfragment 2; TLCK, tosyl-L-lysine chloromethyl ketone; PMSF, phenylmethanesulfonyl fluoride; DTT, dithiothreitol; EDTA, ethylenediaminetetraacetic acid; EtOH, ethanol; R_g, radius of gyration; f_h, fraction helix; SDS, sodium dodecyl sulfate; Da, dalton(s).

melting curves. Twenty minutes was allowed for thermal equilibration at each temperature prior to measurement.

The specific mean residue rotation ($[m']_{231.4}$) was calculated from the specific rotation ($[\alpha]_{231.4}$) by use of the equation:

$$[m']_{231.4} = \frac{3}{n^2 + 2}\frac{M_0}{100}[\alpha]_{231.4} \quad (1)$$

where M_0 is the mean residue molecular weight taken to be 115 and n is the refractive index of the solvent at 231.4 nm. The fraction helix at each temperature was calculated from $[m']_{231.4}$ by using the method of Hvidt et al. (1985) to account for the temperature dependence of the reference state values as follows:

$$f_h(t) = \frac{X - X_c}{X_h - X_c} = \frac{[m']_\lambda(t) - (-1885 - k_c t)}{(-16000 + k_h t) - (-1885 - k_c t)} \quad (2)$$

where X is the observed quantity and t is the temperature (in degrees Celsius). X_h and X_c represent the values of X for the completely helical and random-coil states, respectively, and k_h and k_c are the temperature dependencies of the helix and coil states, respectively. In this study, k_h was determined from the limiting slope of the $[m']_\lambda$ vs temperature plots (λ = 231.4 nm) at low temperature. We found k_h to vary between −48/°C and −62/°C for the rod and its subfragments. A value for k_c = +9/°C was used in all experiments based on the measurements of Hvidt et al. (1985). Protein concentrations were in the range of 0.3–0.5 mg/mL. In previous studies (Stafford, 1985; Tsong et al., 1979), no significant concentration dependence of f_h for rod and its subfragments has been detected.

Light Scattering. A SOFICA 50 photogoniometer was used for elastic light-scattering measurements. Both the incident and scattered beams were unpolarized, and a wavelength of 436 nm was used unless otherwise indicated. Scattered intensities were recorded at 12 angles between 22.5° and 150° with respect to the incident beam.

Samples in 25-mm-diameter cylindrical cells were immersed in a vat filled with a refractive index matching fluid (paraffin oil). The vat fluid was continuously stirred, and the temperature was maintained via an external circulating bath. Melting curves were obtained by ramping the temperature of the vat at a rate of 5 or 10 °C/h. The temperature of the vat was continuously monitored, and the sample temperature was calculated by using previously constructed calibration curves. Measurements were recorded at each scattering angle for every 1- or 2-deg increment in temperature. The maximum change in temperature over the recording period was 0.5 °C. Solvent scattering intensities were found to be nearly independent of temperature, and, therefore, all protein scattering intensities were corrected for solvent scattering at 20 °C.

Scattering cells were rendered dust free according to the method of Godfrey and Eisenberg (1976). Samples (0.1–0.5 mg/mL) were prepared by chromatography on Sephacryl S-300 or S-400. The desired fractions were pooled, centrifuged at 80000g for 2 h, and then filtered under gravity through 0.22-μm Millipore filters directly into the scattering cells. These were allowed to stand overnight at 4 °C prior to measurement.

The light-scattering data were analyzed by nonlinear least-squares fitting of the intensities as a function of θ to the exact $P(\theta)$ form factor for rigid rods:

$$i(\theta) \propto P(\theta) = \frac{2}{qL}\int_0^{qL}\frac{\sin(x)}{x}\,dx - \left[\frac{\sin(qL/2)}{qL/2}\right]^2 \quad (3)$$

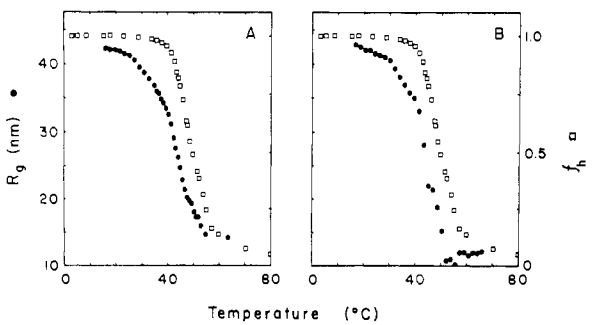

FIGURE 1: Plots of radius of gyration [R_g (●)] and fraction helix [f_h (□)] as a function of temperature for rabbit myosin rod. R_g values were derived from elastic light-scattering measurements as described in the text. f_h values were calculated from optical rotation data according to the method of Hvidt et al. (1985). The protein concentration for the optical rotation melt curve was 0.5 mg/mL. The solvent for both sets of measurements was 0.6 M NaCl, 20 mM phosphate, 1.0 mM EDTA, and 0.5 mM DTT, pH 7.0 (buffer M). (A) R_g values determined at a protein concentration of 0.25 mg/mL. (B) R_g values determined by extrapolating the results of seven melt curves (spanning the concentration range 0.04–0.98 mg/mL) to infinite dilution at each temperature.

where $q = 4\pi n \sin(\theta/2)\lambda_0^{-1}$ and L is the rigid rod length. The radius of gyration is related to L by $R_g^2 = L^2/12$. For values of $qL < 3$, eq 3 above is equivalent to the commonly used approximation

$$i(\theta) \propto 1 - q^2R_g^2/3 \quad (4)$$

See Montague and Newman (1984) for a more detailed discussion.

Gel Electrophoresis. Electrophoresis on SDS gels was carried out according to the method of Laemmli (1970) using a mini slab gel apparatus (Idea Scientific). The acrylamide:methylenebis(acrylamide) ratio was 30:0.8 (w/w). Gels were stained using a 0.25% w/v solution of Coomassie Blue G-250 in methanol/acetic acid/HOH (5:1:5) and destained in methanol/acetic acid/HOH (2:3:35).

RESULTS

Temperature Dependence of f_h and R_g in the Myosin Rod. Figure 1A presents comparative plots of the fraction of helix (f_h) and radius of gyration (R_g) of rabbit myosin rod versus temperature in identical solvents (buffer M). The ordinate scales of these plots have been adjusted so that the two melting profiles roughly coincide at their maximum and minimum values. From our optical rotation data, the fraction of α-helix in the rod was estimated to be about 1.0 (100% helix) at the lowest temperature measured (~2 °C) and remains essentially unchanged on gradually increasing the temperature to ~35 °C. Above this point, f_h drops rapidly with temperature, leveling off at about 80 °C near 0% helical structure ($f_h \simeq$ 0.05). Derivative plots, $d(f_h)/dt$, of this curve reveal the presence of at least two separate and distinct melting phases (Burke et al., 1973; Tsong et al., 1983), a feature characteristic of multidomain structures as shown by the work of Potekhin et al. (1979) and reviewed by Privalov (1982). The midpoint of the overall melting curve under the ionic conditions of buffer M was 49 °C.

The R_g vs T curve is displaced with respect to the corresponding f_h vs T plot to lower temperatures by about 5 °C. As the temperature is increased above 20 °C, the radius of gyration drops continuously until it reaches a value of ~15 nm near 50 °C. It will be noted that a substantial drop in R_g occurs in the temperature range 20–35 °C where f_h is essentially invariant. This result is a good indication that myosin

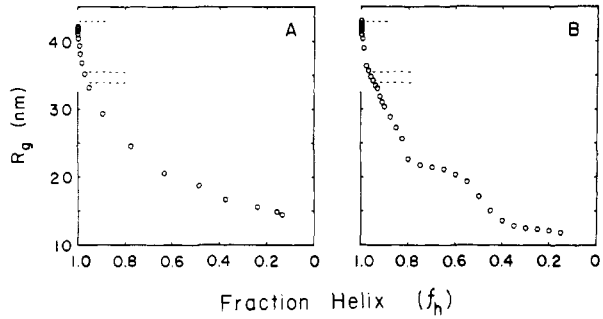

FIGURE 2: Radius of gyration vs fraction helix for rabbit myosin rod. The data from Figure 1 have been replotted, eliminating the temperature axis to show the correlation between radius of gyration (R_g) and fraction helix (f_h). Points were obtained at 2.5-deg increments between 15 and 55 °C by interpolation along smooth curves drawn through the melting profiles. The maximum observed radius of gyration (~43 nm) corresponds to a rigid rod length of 150 nm and is indicated by the upper dashed line. The calculated R_g values for a rod of this length hinged either at its center or at a point located at one-third of the length are marked with dashed lines (lower and middle, respectively). (A) Data from Figure 1A. (B) Data from Figure 1B.

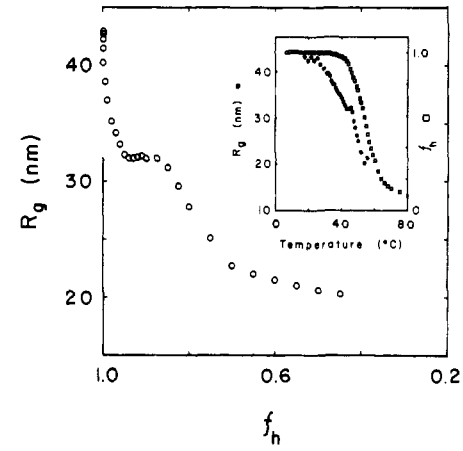

FIGURE 3: Radius of gyration vs fraction helix for myosin rod in solvent A. A plot of radius of gyration vs fraction helix for myosin rod in 0.5 M KCl, 0.5 M potassium phosphate, 1 mM EDTA, and 1 mM DTT, pH 7.3 (buffer A), is shown. Points were obtained by the same method described in Figure 2. In this very high ionic strength solvent, we observed the same initial drop in R_g vs f_h as seen in Figure 2. R_g then remains nearly constant at ~34 nm until f_h has reached 0.85. Further decreases in f_h are accompanied by a more gradual drop in R_g. Inset: The observed R_g and f_h vs temperature curves. The midpoint of the f_h vs t plot is shifted to ~56 °C in this solvent system, and the R_g vs t curve is also shifted to higher temperatures. In addition, a small but distinct discontinuity is observed in the light-scattering melt curve between 43 and 46 °C. R_g is essentially invariant over this temperature range. Protein concentrations were 0.5 and 0.22 mg/mL for the optical rotation and light-scattering melting curves, respectively.

rod is flexible and has swivel joints.

R_g extrapolates to a value of about 43 nm at low temperature. Assuming a rigid rod model, we estimate a length of ~149 nm at temperature between 10 and 20 °C, consistent with values of 155 ± 4 nm, based on electron microscope studies of rabbit myosin rod (Elliott & Offer, 1978; Walker et al., 1985). This estimate is only slightly smaller than the length calculated for an α-helical strand of 1100 residues (rat myosin rod; Strehler et al., 1986) in a coiled-coil structure assuming a pitch of 1.5 Å/residue.

Earlier studies have shown that myosin rod can self-associate to form a parallel dimer with axial displacement of 43 nm (Harrington & Burker, 1972). Since R_g obtained from light scattering is a z-average parameter, it is sensitive to small amounts of dimer present in solution. To check on the possibility that the shift in the melting profiles of Figure 1A might be related to the presence of dimer molecules, light-scattering melting curves were determined at seven different protein concentrations over the range 0.04–0.98 mg/mL. The R_g calculated at each temperature from these profiles was extrapolated to $c = 0$, and these values are plotted in Figure 1B. It is clear from a comparison of panels A and B of Figure 1 that the difference in the R_g and f_h melting profiles is not dependent on the presence of dimer but rather stems from a structural transition in the monomeric myosin rod.

To obtain a better understanding of the relationship between f_h and R_g, the data in Figure 1 have been replotted to eliminate the temperature axis. Figure 2 shows plots of R_g vs f_h for myosin rod, where the points were obtained by interpolation of the curves in Figure 1 at various temperatures between 20 and 60 °C. Here we see that a decrease in helical content of only a few percent from the low-temperature value, $f_h = 1.0$, is accompanied by a marked drop in radius of gyration (from $R_g = 43$ to ~35 nm). The initial stage of the melting process is followed by a more gradual fall in R_g with increasing helix–coil melting within the rod structure.

In earlier enzyme probe studies of the myosin rod and isolated S-2 subfragments (Ueno & Harrington, 1984a,b), we found that at temperatures between 5 and 25 °C local melting is confined to a restricted segment within the S-2 region near the LMM/HMM junction. At temperatures between 25 and 40 °C, proteolytic cleavage spreads to several sites throughout the S-2 hinge domain, with the center of this structural region showing the largest increase in local site melting. The data of Figure 2 appear to be consistent with initial local melting and hinging of the rod near the LMM/HMM junction, i.e., at a locus about 73 Da per chain (~95 nm) from the C-terminus of the rod. Additional melting in the hinge region appears to be responsible for the gradual drop in R_g vs f_h up to temperatures of ~40 °C ($f_h \cong 0.95$).

The melting profile of the myosin rod is known to be dependent on the ionic conditions of the solvent (Stafford, 1985). With increasing ionic strength, the melt curve is shifted to higher temperatures, and individual melting domains are translated to different extents along the temperature axis. The R_g vs f_h profile of the rod in such a high ionic strength solvent (solvent A) is presented in Figure 3. Again, we see a dramatic drop in R_g in the early stages of melting under these ionic conditions and before any significant change occurs in the α-helical content of the structure. This process is followed by a nearly invariant R_g as the double α-helix undergoes additional melting down to $f_h \cong 0.85$. Beyond this point, R_g declines gradually as the structure undergoes further melting.

The plateau seen in the R_g vs f_h plot is a reflection of the discontinuity observed in the R_g vs t melting profile between 42 and 46 °C (inset, Figure 3). This behavior is consistent with the increased stabilization with increasing ionic strength of the rod segments flanking the hinge domain (LMM and short S-2) which is observed in enzyme probe studies (Ueno & Harrington, 1984b). The hinge domain is relatively insensitive to ionic strength.

Temperature Dependence of f_h and R_g in LMM and S-2 Subfragments. In this section, we examine the melting behavior of the constituent elements of the rod, LMM and long S-2, prepared by proteolytic cleavage at the LMM/HMM junction. Figures 4 and 5 show R_g and f_h versus temperature plots for LMM and long S-2 subfragments scaled as in Figure 1 to allow easy comparison of the melting curves. It is clear that, unlike the rod, the R_g and f_h versus temperature profiles are virtually superimposable for both subfragments over the

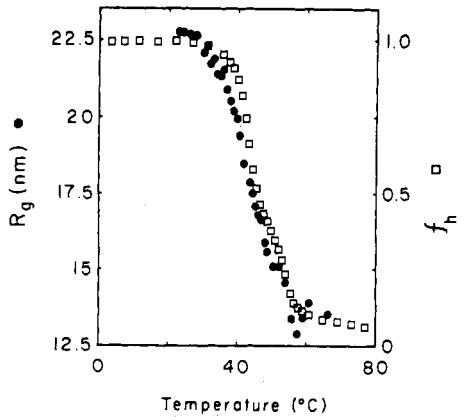

FIGURE 4: Radius of gyration (R_g) and fraction helix (f_h) vs temperature for LMM. The radius of gyration (●) and fraction helix (□) as a function of temperature are shown for LMM. Data were obtained in the same manner as in Figure 1. The estimated rigid rod length at low temperature is 79 nm which is slightly larger than the length of 74 nm for LMM observed in electron microscope studies (Walzthöny et al., 1986). Unlike myosin rod, the R_g and f_h melting profiles are nearly superimposable. Buffer M was the solvent in these experiments. Protein concentrations were 0.27 and 0.68 mg/mL for the optical rotation and light-scattering melting curves, respectively.

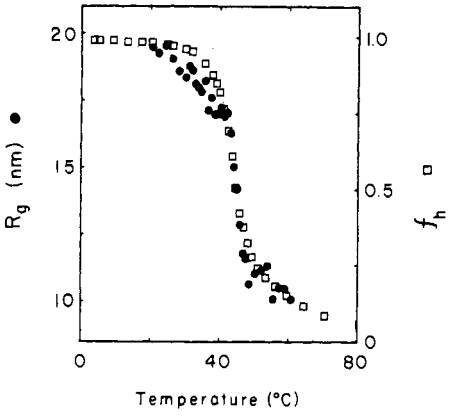

FIGURE 5: Radius of gyration (R_g) and fraction helix (f_h) vs temperature for long S-2. Plots of R_g (●) and f_h (□) versus temperature are shown for long S-2. Data were obtained in the same manner as in Figure 1. Between 20 and 38 °C, the decrease in R_g slightly precedes the drop in f_h. Between 38 and 41 °C, R_g is virtually unchanged with a value of 17 nm. At higher temperatures, the changes in R_g and f_h are directly proportional. The estimated rigid rod length at low temperatures is 67 nm which compares well with 69 nm observed in recent electron microscope studies (Walzthöny et al. 1986). These experiments were carried out in buffer M. Protein concentrations were 0.14 and 0.12 mg/mL for the optical rotation and light-scattering experiments, respectively.

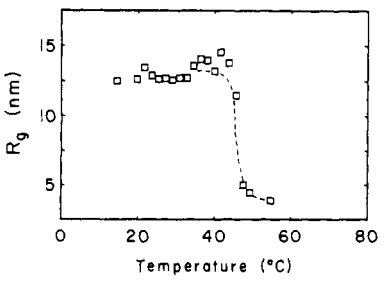

FIGURE 6: Radius of gyration vs temperature for short S-2. The radius of gyration (R_g) has been measured as a function of temperature for short S-2 in buffer M. Since the dissymmetry of short S-2 is relatively low, the studies were carried out at a wavelength of 365 nm. Unlike long S-2, short S-2 shows virtually constant R_g (~12.8 nm) vs temperature up to 45 °C. Above this temperature, R_g drops over a very narrow temperature range to a value of ~4 nm. These results allow us to correlate the gradual change in R_g of long S-2 between 20 and 40 °C with melting in the hinge region.

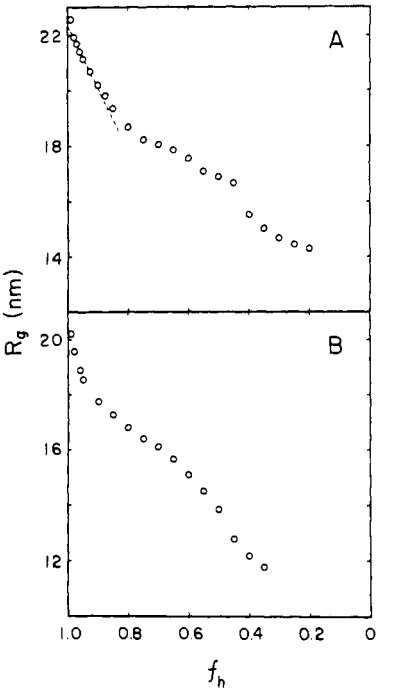

FIGURE 7: Radius of gyration vs fraction helix for LMM and long S-2. The data in Figures 5 and 6 have been combined to eliminate the temperature axis. Points were estimated by the method described in Figure 2. (A) R_g vs f_h for LMM. (B) R_g vs f_h for long S-2. Unlike myosin rod, neither LMM nor long S-2 shows the precipitous drop in R_g at very high values of f_h. Rather, R_g and f_h appear to change gradually in direct proportion. The dashed line in (A) indicates the expected curve if R_g is directly proportional to f_h.

entire melting range, indicating that the radius of gyration and hence the apparent length of these two coiled-coil α-helical structures are directly proportional to the fraction helix. This finding provides strong support for our earlier conclusion that the myosin rod undergoes hinging near its center at temperatures between 25 and 35 °C.

Unlike LMM, the early phase of melting in long S-2 does show a region where the R_g vs temperature plot begins a perceptible decline slightly ahead of the f_h vs temperature profile (Figure 5). This behavior probably results from melting in the hinge region which, following proteolytic cleavage of the rod at the LMM/HMM junction, now occupies about one-third (~150 residues per chain) of the long S-2 structure at its C-terminal end. It is known from scanning calorimetric (Swenson & Ritchie, 1980) and proteolytic digestion studies (Ueno & Harrington, 1984b) that this region has a lower thermal stability than the flanking short S-2 and LMM segments of the rod. Our interpretation of the long S-2 melting curve is supported by the R_g vs temperature melting curves of short S-2 (Figure 6). This subfragment, which is devoid of the hinge region, shows no change in radius of gyration with increasing temperature up to 45 °C.

Plots of R_g vs f_h for both LMM and long S-2, presented in Figure 7, reflect the markedly different melting behavior of these two structures as compared to myosin rod. The dashed line shows the expected dependence of R_g on f_h if initial melting is occurring from the ends of these structures rather than from a central domain (i.e., R_g should be proportional to f_h) and is seen to give a good approximation of the melting behavior of LMM in the early phases of this process.

Discussion

In this paper, we have examined the question of hinging within the myosin rod by correlating changes in the secondary

structure as measured by optical rotation with changes in the overall conformation as measured by elastic light scattering. This approach provides a more complete picture of the solution behavior of myosin rod than is obtained by using a single method and allows us to explain some of the apparently contradictory results on the question of hinging in the literature.

At temperatures below 20 °C in buffer M and 25 °C in buffer A, myosin rod clearly behaves as an extended rodlike molecule. The estimated rigid rod length is consistent with values observed in the electron microscope and is only slightly smaller than the calculated length based on a 100% α-helix assuming 1100 residues per chain (Strehler et al., 1986). Thus, any measurements of the particle asymmetry made at low temperatures would not detect hinging in the myosin rod.

Between 20 and 40 °C, a marked decrease in the radius of gyration is observed, while only a small change is detected in the fraction helix. At 40 °C, the radius of gyration has dropped to about $(5/8)^{1/2}$ of the low-temperature value, a result consistent with hinging of the myosin rod near its center [see Yu and Stockmayer (1967)]. If we assume the location of the hinge to be at a point one-third of the length from the end of the rod (i.e., at the end of the short S-2), we calculate an R_g of $(55/81)^{1/2}$ of the rigid rod value. This is only 4% larger than the expected R_g for a central hinge. For a 150-nm rod, these two hinge positions yield calculated R_g's of 35.5 nm (one-third hinge) and 34 nm (central hinge). It seems likely, therefore, that the mechanical hinge is located within the proteolytically sensitive hinge region (Ueno & Harrington, 1984a).

As the temperature is increased further, R_g and f_h change in direct proportion up to about 50 °C. LMM, on the other hand, shows no such discontinuity in plots of R_g vs f_h. In this case, the change in radius of gyration is directly proportional to the change in fraction helix over the temperature range 20–40 °C. Similar results have been obtained for long S-2. In this case, however, during the earliest stages of melting, the drop in R_g slightly precedes the drop in f_h, suggesting melting in the hinge region which comprises the C-terminal one-third of long S-2.

Earlier studies using elastic light scattering as a function of temperature have failed to detect significant hinging in myosin rod (Hvidt et al., 1984). In those studies, the radius of gyration of myosin rod in buffer A was measured between 7 and 43 °C and found to be ~38 nm at all temperatures, a value somewhat lower than the low-temperature value found in this study. The reason for the discrepancy is not clear but may be due to differences in the analysis of the data. We have analyzed our data using the complete $P(\theta)$ function for a rigid rod whereas Hvidt et al. used the standard one-term linear approximation for intensity vs $\sin^2(\theta/2)$ to estimate R_g (eq 2). This approximation is generally not valid for long rods at high scattering angles and will lead to a low estimate for R_g. Second, all of our data were collected over an angular range of 30–150° while the data used in the previous study covered only 50–130°. The wider data range used in this study allows a more accurate estimate of the radius of gyration of these particles.

Derivative plots of the optical rotation melting profiles of myosin rod in buffer M and in buffer A (not shown) have two clearly resolved peaks. Analysis of these plots allows one to estimate the amount of structure undergoing melting and the apparent mean residue enthalpy (ΔH^{res}_{app}) in each transition. Comparison of the ΔH^{res}_{app} with the calorimetric enthalpy (ΔH^{res}) provides an estimate of the number of domains melting in each observed optical rotation transition. Potekhin et al. (1979) find a calorimetric ΔH^{res} value of ~1800 J mol^{-1} for myosin rod fragments under similar solvent conditions. In buffer M, the 55 °C transition contains ~20% of the structure and has a ΔH^{res}_{app} of 1766 J mol^{-1}. This correlates well with transition V of Potekhin et al. (1979) which contains 17% of the structure and has a ΔH^{res} of 1790 J mol^{-1}. The lower transition (47 °C) has a ΔH^{res}_{app} of 270 J mol^{-1} and contains about 60% of the structure. Thus, several domains are likely to be melting in this transition. In buffer A, we observe two transitions, one at 47 °C and one at 57 °C with respective fractions of 18% and 69%. Clearly, much of the structure has been stabilized in this high ionic strength solvent. The low-temperature transition probably represents melting in the hinge region which is known to have little ionic strength dependence (Ueno & Harrington, 1984b; Stafford, 1985). This is also consistent with the R_g vs f_h data in Figure 3 where no change in R_g was observed over the f_h range of 0.98–0.85. The ΔH^{res}_{app} of this transition is 980 J mol^{-1}, suggesting that only one or two domains are involved. The 57 °C transition has a ΔH^{res}_{app} of ~200 J mol^{-1}, suggesting several domains are involved in this transition.

Our results clearly indicate hinging of myosin rod at temperatures between 20 and 40 °C. Two recent electron microscopy studies of myosin and myosin rod support this conclusion. Walker and Trinick (1986) and Walzthöny et al. (1986) have measured the length of myosin rod as a function of temperature in the electron microscope. Both groups find that between 20 and 40 °C, myosin rod shortens and the principle site of melting is in the "hinge"region. The physical properties of the rod are quite dependent on both temperature and solvent conditions. The apparent discrepancies in previous studies may well be due to the choice of experimental conditions. The physiological significance of the hinge in myosin rod is not clear, but it has been incorporated to different extents into various models of contraction (Huxley, 1969; Huxley & Simmons, 1971; Harrington, 1971, 1979). It is difficult to extrapolate directly from the solution properties of myosin rod to its behavior in the organized thick filament. Nevertheless, enzyme probe studies (Ueno & Harrington, 1986a,b) show a marked decrease in the structural stability of the hinge region upon activation. These results indicate a significant modulation of the properties of the hinge within the organized filament during the cross-bridge cycle and suggest an important role for the hinge region in the contractile process.

ACKNOWLEDGMENTS

We thank Howard Flaxman for excellent technical assistance. We are also grateful to Drs. Søren Hvidt and Francis Carlson for many helpful discussions.

REFERENCES

Bernengo, J. C., & Cardinaud, R. (1982) *J. Mol. Biol. 159*, 501–517.

Burke, M., Himmelfarb, S., & Harrington, W. F. (1973) *Biochemistry 12*, 701–710.

Elliott, A., & Offer, G. (1978) *J. Mol. Biol. 123*, 505–519.

Godfrey, J. E., & Harrington, W. F. (1970) *Biochemistry 9*, 886–893.

Godfrey J. E., & Eisenberg, H. (1976) *Biophys. Chem. 5*, 301–318.

Harrington, W. F. (1971) *Proc. Natl. Acad. Sci. U.S.A. 68*, 685–689.

Harrington, W. F. (1979) *Proc. Natl. Acad. Sci. U.S.A. 76*, 5066–5070.

Harrington, W. F., & Burke, M. (1972) *Biochemistry 11*, 1448–1455.

Harvey, S. C., & Cheung, H. C. (1977) *Biochemistry 16*, 5181–5187.
Harvey, S., & Cheung, H. C. (1982) *Cell Muscle Motil. 2*, 279–302.
Highsmith, S., Kretzschmar, K. M., O'Konski, C. T., & Morales, M. F. (1977) *Proc. Natl. Acad. Sci. U.S.A. 74*, 4986–4990.
Huxley, A. F., & Simmons, R. M. (1971) *Nature (London) 233*, 533–538.
Huxley, H. E. (1969) *Science (Washington, D.C.) 164*, 1356–1366.
Hvidt, S., Nestler, F. H. M., Greaser, M. L., & Ferry, J. D. (1982) *Biochemistry 21*, 4064–4073.
Hvidt, S., Chang, T., & Yu, H. (1984) *Biopolymers 23*, 1283–1294.
Hvidt, S., Rodgers, M. E., & Harrington, W. F. (1985) *Biopolymers 24*, 1647–1662.
Laemmli, U. K. (1970) *Nature (London) 227*, 680–685.
Lu, R. C., & Wong, A. (1985) *J. Biol. Chem. 260*, 3456–3461.
Mihalyi, E., & Harrington, W. F. (1959) *Biochim. Biophys. Acta 36*, 447–466.
Montague, C. E., & Newman, J. (1984) *Macromolecules 17*, 1391–1396.
Potekhin, S. A., Trapkov, V. A., & Privalov, P. L. (1979) *Biofizika 24*, 46–50.
Privalov, P. L. (1982) *Adv. Protein Chem. 35*, 1–104.
Rosser, R. W., Nestler, F. H. M., Schrag, J. L., Ferry, J. D., & Greaser, M. (1978) *Macromolecules 11*, 1239–1242.
Shaw, E., Mares-Guia, M., & Cohen, W. (1965) *Biochemistry 4*, 2219–2224.
Stafford, W. F., III (1985) *Biochemistry 24*, 3314–3321.
Strehler, E. E., Strehler-Page, M.-A., Perriard, J.-C., Periasamy, M., & Nadal-Ginard, B. (1986) *J. Mol. Biol. 190*, 291–318.
Sutoh, K., Sutoh, K., Karr, T., & Harrington, W. F. (1978) *J. Mol. Biol. 126*, 1–22.
Swenson, C. A., & Ritchie, P. A. (1980) *Biochemistry 19*, 5371–5375.
Takahashi, K. (1978) *J. Biochem. (Tokyo) 83*, 905–908.
Tsong, T. Y., Karr, T., & Harrington, W. F. (1979) *Proc. Natl. Acad. Sci. U.S.A. 76*, 1109–1113.
Tsong, T. Y., Himmelfarb, S., & Harrington, W. F. (1983) *J. Mol. Biol. 164*, 431–450.
Ueno, H., & Harrington, W. F. (1984a) *J. Mol. Biol. 173*, 35–61.
Ueno, H., & Harrington, W. F. (1984b) *J. Mol. Biol. 180*, 667–701.
Ueno, H., & Harrington, W. F. (1986a) *J. Mol. Biol. 190*, 59–68.
Ueno, H., & Harrington, W. F. (1986b) *J. Mol. Biol. 190*, 69–82.
Ueno, H., Rodgers, M. E., & Harrington, W. F. (1983) *J. Mol. Biol. 168*, 207–228.
Walker, M., & Trinick, J. (1986) *J. Mol. Biol. 192*, 661–667.
Walker, M., Knight, P., & Trinick, J. (1985) *J. Mol. Biol. 184*, 535–542.
Walzthöny, D., Eppenberger, H. M., Ueno, H., Harrington, W. F., & Wallimann, T. (1986) *Eur. J. Cell. Biol. 41*, 38–43.
Yu, H., & Stockmayer, W. (1967) *J. Chem. Phys. 47*, 1369–1373.

Thermal Stability of Myosin Rod from Various Species†

M. E. Rodgers,* T. Karr, K. Biedermann,‡ H. Ueno,§ and W. F. Harrington
Department of Biology and McCollum-Pratt Institute, The Johns Hopkins University, Baltimore, Maryland 21218
Received November 3, 1986; Revised Manuscript Received August 24, 1987

ABSTRACT: The radius of gyration and fraction helix as a function of temperature have been determined for myosin rod from four different species: rabbit, frog, scallop, and antarctic fish. Measurements from sodium dodecyl sulfate gel electrophoresis indicate that all particles have the same molecular weight (~130K). All fragments are nearly 100% α-helical at low temperatures (0–5 °C). The melting profiles for each are qualitatively similar in shape, but their midpoints are shifted along the temperature axis in the following order: antarctic fish (T_m = 33 °C), scallop (T_m = 39 °C), frog (T_m = 45 °C), and rabbit (T_m = 49 °C). Corresponding radius of gyration vs temperature profiles for each species are shifted to lower temperatures (approximately 5–8 °C) with respect to the optical rotation melting curves. From plots of radius of gyration vs fraction helix, we find a marked drop in the radius of gyration (from 43 to ~34 nm) with less than a 5% decrease in fraction helix for rabbit, frog, and antarctic fish rods, whereas the radius of gyration of scallop rod never exceeds 34 nm. Results indicate hinging of the myosin rod of each species. The thermal stabilities of the myosin rods shift in parallel with the working temperature of their respective muscles.

In the preceding paper (Rodgers & Harrington, 1987), we have combined light-scattering and optical rotation measurements to provide evidence for a flexible region, the light meromyosin–heavy meromyosin hinge (LMM–HMM hinge),[1] in rabbit myosin rod. Hinges in myosin rod have also been clearly demonstrated in smooth muscle myosin using both electron microscopy and analytical centrifugation (Trybus et

† Supported by National Institutes of Health Grant AM-04349 (to W.F.H.) and by a Muscular Dystrophy Association postdoctoral fellowship (to M.E.R.). This is Contribution No. 1387 of the McCollum-Pratt Institute.
* Address correspondence to this author at the Department of Biology, The Johns Hopkins University.
‡ Present address: Institute of Biotechnology, The Technical University of Denmark, DK-2800 Lyngby, Denmark.
§ Present address: Corporate Research and Development, Ube Research Lab, Ube Industries, Ltd., Ube-shi, Yamaguchi-ken, 755 Japan.

[1] Abbreviations: S-1, myosin subfragment 1; LMM, light meromyosin; HMM, heavy meromyosin; TLCK, tosyl-L-lysine chloromethyl ketone; PMSF, phenylmethanesulfonyl fluoride; IAA, iodoacetic acid; EDTA, ethylenediaminetetraacetic acid; DTT, dithiothreitol; R_g, radius of gyration; f_h, fraction helix; SDS, sodium dodecyl sulfate.

0006-2960/87/0426-8703$01.50/0